Microstructure Change of SOFC Anode Caused by Electrochemical Redox Cycles

Norikazu Takagi, Yoshinori Nakamura, Naoki Shikazono and Nobuhide Kasagi

The University of Tokyo, Department of Mechanical Engineering
Hongo 7-3-1, Bunkyo-ku, Tokyo 113-8656, Japan
Tel.: +81-03-5841-6419
Fax: +81-03-5800-6999
ntakagi@thtlab.t.u-tokyo.ac.jp

Abstract

During SOFC operation with typical Ni-YSZ anode, Ni is always subjected to the risk of oxidation. For example, local steam partial pressure can be high near the three phase boundary (TPB) at large current density operations, and unexpected fuel interruption can increase oxygen partial pressure. Although the effect of redox cycles on anode performance has been intensively investigated, quantitative change of anode microstructure caused by oxidation and reduction (redox) cycles is still unclear. In this study, electrochemical redox cycling was imposed on typical electrolyte support cell, and the anode microstructures before and after redox cycling were reconstructed using dual beam focused ion beam scanning electron microscope (FIB-SEM) technique. Then, statistical parameters such as TPB density, particle diameter and tortuosity factor were calculated. In addition, overpotential was calculated by the lattice Boltzmann method (LBM) simulation and compared with the experiment result.

1. Introduction

SOFC is one of the most promising technologies for future energy systems due to its high efficiency and fuel flexibility. Materials, cell/stack/system designs have been improved by intensive researches from various fields such as chemistry, electrochemistry, mechanical engineering, material science and so on.

In the Ni/YSZ porous anode, electrode reaction takes place at the interface of ionic, electronic and gaseous conducting phases, so evaluation of three phase boundary (TPB) density and phase connectivities are very important for performance improvement. During SOFC operation with typical Ni-YSZ anode, Ni is always subjected to the risk of oxidation. For example, local steam partial pressure can be high near the TPB at large current density operations, and unexpected fuel interruption can increase oxygen partial pressure. Although the effect of redox cycles on anode performance has been intensively investigated [1][2][3], quantitative change of anode microstructure caused by oxidation and reduction (redox) cycles is still unclear. In this study, electrochemical redox cycling[4] was imposed on typical electrolyte support cell, and the anode microstructures before and after redox cycling were reconstructed using dual beam focused ion beam scanning electron microscope (FIB-SEM) technique[6]. Then, statistical parameters such as TPB density, particle diameter and tortuosity factor were calculated. In addition, Overpotential was calculated by the lattice Boltzmann method (LBM)[7] and compared with the experimental result.

2. Experimental

2.1 Cell fabrication

Electrolyte-support Ni/YSZ anode was made by screen printing and sintering processes. Original powder of NiO;YSZ=60;40 composite was screen printed on polished dense YSZ disk with thickness of 0.5 mm and diameter of 20 mm. Anode was sintered at 1400 ^{o}C for 3 hours, and cathode at 1150 ^{o}C for 3 hours. Thicknesses of anode and cathode are 30 μm and 10 μm, respectively. Pt wire was winded around the side of YSZ disk with Pt paste as a reference electrode.

2.2 Electrochemical oxidation

Electrolyte supported planer cell was tested in high temperature furnace shown in Fig.1. Cell is put between alumina tubes and sealed by pylex glass ring. Platinum meshes touch on surfaces of electrodes as current collectors.

Experimental procedure is shown in Fig.2. Anode was initially reduced by hydrogen at 800 ^{o}C. As the standard operation condition, 50ccm hydrogen with 3% steam was supplied to the anode, and 50ccm pure oxygen to the cathode. Using Solartron 1255WB, IV curves were measured by sweeping the voltage at the rate of 4 mV/sec. Impedance spectroscopy were conducted at bias current of 0 (OCV), 0.05, 0.10, 0.15, 0.20, 0.25, 0.30 A/cm^2. Applied frequency was from 10^0 to 10^5 Hz, and amplitude was 10mV at OCV and 10% of applied bias current. Impedance plot was fitted to equivalent circuit shown in Fig.3 using Zplot to obtain impedance values at each bias current.

Ohmic overpotential is defined as; $\eta_{ohm} = \int R_{ohm}(I)dI$. Reaction overpotential η_{reac} is defined as $\eta_{reac} = \eta_{act} + \eta_{conc}$, which was calculated by subtracting ohmic overpotential from total overpotential obtained from the IV measurement.

Imitating the fuel shortage situation in practical use, nickel was oxidized by the ionic current under nitrogen atmosphere. After anode gas was changed from hydrogen to 50sccm dry nitrogen (Experiment A) or 50sccm 20% humidified nitrogen (Experiment B), 10 mA/cm^2 current was applied until voltage fell sharply as shown in Fig.4. In the initial period 1, remained hydrogen gas was consumed, and then nickel was oxidized in period 2. The reaction is expressed as Ni+O^{2-} → NiO+2e$^-$. Total amount of charge is about 9C during each redox cycle, which corresponds to oxidation of 20% of total nickel in the anode. Then, oxidized anode was held in 3% humidified hydrogen for 30min as a re-reduction

step. This redox cycle was repeated twice. Measurement of IV curve and impedance were repeated in-between the redox cycles. In order to separate the effects of electrochemical oxidation and water[5], initially reduced anode was exposed to 20% humidified nitrogen for 1 hour and then held in 3% humidified hydrogen without current load (Experiment C). As for comparison, NiO-YSZ anode was cooled down just after the initial reduction step (Experiment X). Experimental conditions are summarized in Table 1.

2.3 Three dimensional reconstruction

  Three-dimensional reconstruction is conducted in the same manner reported in Ref. [6]. Anode sample was infiltrated by resin, then hand polished, and finally polished by Ar-ion beam cross-section polisher (JEOL Ltd., SM-09010). To avoid drift phenomenon caused by charging of non-conductive compositions, carbon layer of 4nm was deposited on polished surface and carbon paste was put between the metal block support and the carbon layer. Carbon layer of 0.2 μm thickness was coated on the target region to make the surface smoother. Using FIB-SEM (NVison40, Carl Zeiss), polished surface was pre-milled and successive cross-section SEM images were obtained, as shown in Fig. 5. Alignment of SEM images was corrected, and three phases of pore, YSZ and nickel were separated based on their gray scales. Identification of the phases in SEM images was confirmed by EDX analysis.

  From the reconstructed microstructures, static parameters of anode microstructures were calculated. Connectivity was defined as the ratio of the connected volume from the edge plane to the total volume of the corresponding phase. Connectivity from six edge planes can be defined, and the average and the standard deviation of these values were calculated. Particle and pore diameters were defined as the maximum sphere diameter included in the phase. Ni-YSZ interface area was obtained by the marching cube method[8]. TPB density was obtained by the centroid method [6,7]. Tortuosity factor τ was obtained by solving diffusion equations using the lattice Boltzmann method [7].

3. Numerical simulation

  The gaseous, ionic and electronic transport equations coupled with electrochemical reaction at TPB in the reconstructed three-dimensional microstructure is solved using the lattice Boltzmann method. Details of the calculation method are described in our previous paper[7].

4. Results

4.1 Overpotential

  In experiments A and C, measured overpotentials remained nearly unchanged, while it increased in experiment B as shown in Figs. 6, 7 and 8.

4.2 Microstructures

  Figure 9 shows the SEM images of the original (X) and the anodes after experiments (A), (B) and (C). After experiment A, Ni particles became larger and its surface became smoother. In addition, micro cracks in YSZ particles are marked by white arrows, which are caused by the volume expansion during Ni oxidation. These cracks were not observed in the other experiments. In the experiment B, Ni particle became smaller and more rounded.

  From successive SEM images, microstructures of $23.8\times13.0\times12.8\mu m^3$ were reconstructed for the cells before and after the experiments. The pixel size of each image was 37nm, and the distances between the images were 72.0 nm, 52.6 nm and 41.4 nm for experiments A, B and C, respectively. Then, the microstructures were converted to 100 nm cubic voxels for the subsequent LBM calculation.

  Figure 10 shows volume fraction of the three phases. The ratio is almost unchanged throughout the experiments. Figure 11 shows the volume ratio of YSZ and Ni, which is

nearly the same as the volume ratio of original powders. Therefore, it confirmed that the three-phase separation process was conducted reliably.

Figure 12 shows the comparison of the connectivity of each phase. The bars indicate standard deviations for six directions. In Experiment B, Ni connection was degraded substantially, while Ni remained connected quite well in experiments A and C.

Ni and YSZ particle diameters are shown in Figs. 13 and 14. Ni diameter became lager after redox cycles. It became the largest after experiment A, and it was the second after experiment B. On the other hand, YSZ particle size remained unchanged for all experiments.

Active TPB density of experiment B cell is very small as shown in Fig. 15. However, in terms of total TPB density, experiment A showed the lowest value. This result can be explained by Ni particle diameter and Ni-YSZ interface area shown in Fig.16. In the case of experiment A, Ni particle purely expanded during oxidation and broke the contact between Ni and YSZ. On the other hand, in experiment B, Ni particle became small while Ni-YSZ interface area remained nearly unchanged.

Tortuosity factor is shown in Fig.17. In the pore and YSZ phases, the differences between the samples are relatively small. Ni tortuosity factor in experiment B could not be calculated because Ni phase was not connected from one edge to the other. Such a structural characterization of degraded Ni connection and loss of TPB density can explain the performance degradation. On the other hand, in experiment C, where current load was not applied, structural parameters remained nearly unchanged.

4.3 Overpotential calculation

Calculated overpotentials are compared with the experimental results in Fig. 18. Overpotential of experiment A is larger than the original (X), but the difference is relatively small. On the other hand, Overpotential of experiment B is much larger than the original. The trend of numerical results is qualitatively consistent with the experimental data, so the degradation of cell performance can be basically attributed to the microstructural change.

5. Conclusion

Details of microstructural changes of Ni/YSZ anode before and after electrochemical redox cycles were investigated through 3D reconstruction. It was revealed that presence of steam during redox cycles largely affects the microstructural change.

Such a structural characterization of degraded Ni connection and decrease of TPB density can explain the increase of anode overpotential. The cause of the structural degradation should be attributed to the combined effect of high steam concentration and electrochemical oxidation.

Acknowledgement

References

[1] D. Sarantaridis and A. Atkinsin, *Fuel Cells*, 7 (2007), 246–258.
[2] A. Grauche et al., *ECS Transactions*, 25 (2009), 411-419.
[3] D. Sarantaridis et al., *J. Power Sources*, 180 (2008), 704–710.
[4] T. Hatae et al., *Solid State Ionics*, 179 (2008), 274-281.
[5] A. Gubner et al., *Proceedings 5th Int. Symp. on SOFC*, (1997), 844-850.
[6] H. Iwai et al., *J. Power Sources*,195 (2010) 955–961.
[7] N. Shikazono et al., *J. Electrochem. Soc.*, 157 (2010), B665-B672.
[8] W. E. Lorensen and H. E. Cline, *Computer Graphics*, 21 (1987), 163-169.

Table 1   Experimental condition.

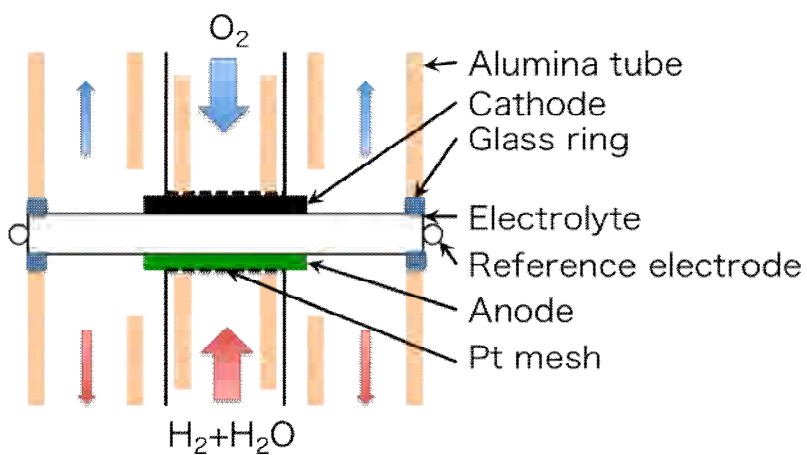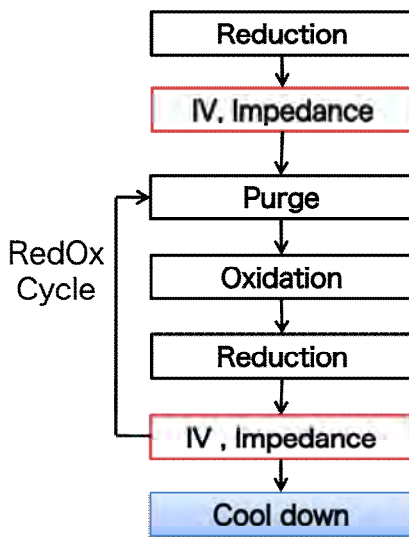| Sample	Condition
A	Electrochemical redox in dry N_2
B	Electrochemical redox in humidified N_2
C	Held in humidified N_2 without current load
X	Original

Fig.1   Experimental setup.
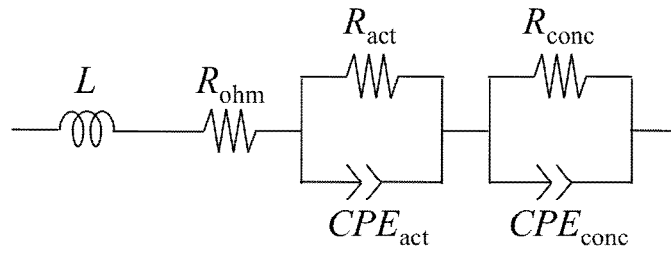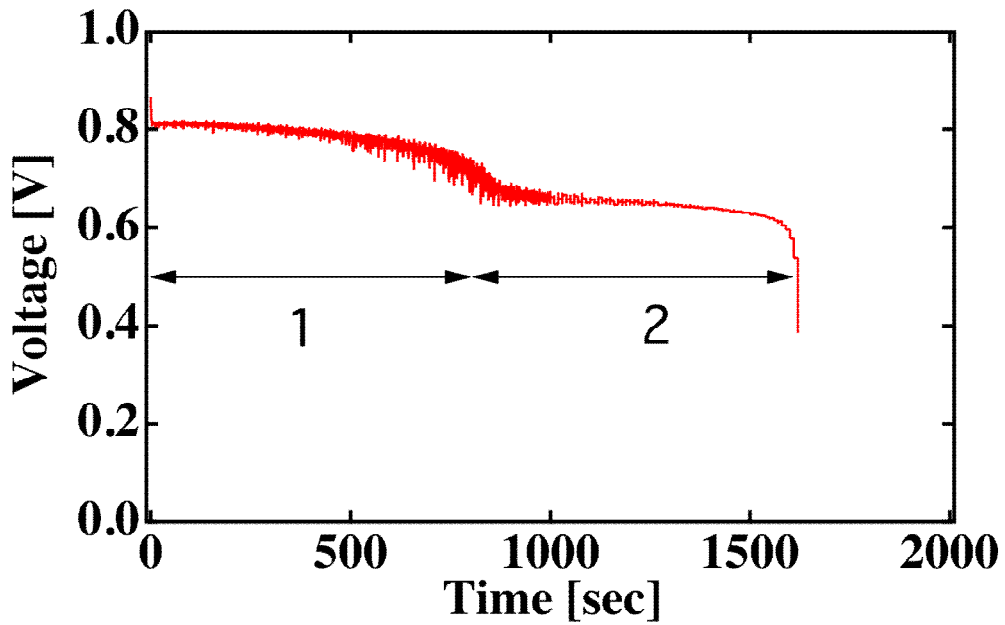

Fig.2   Flow chart of the Redox experiment.

Fig.3 Equivalent circuit of the anode.

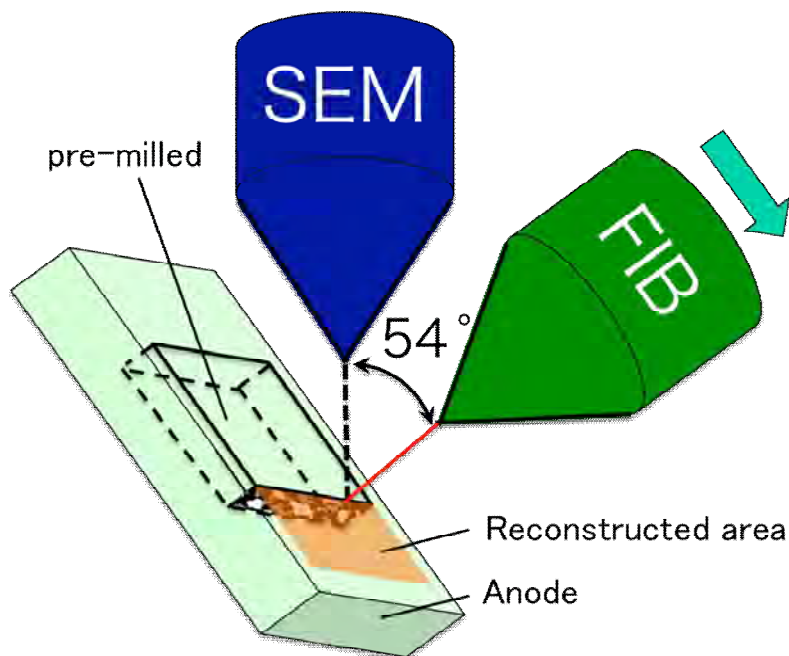Fig.4 Time variation of measured voltage during nickel oxidation.
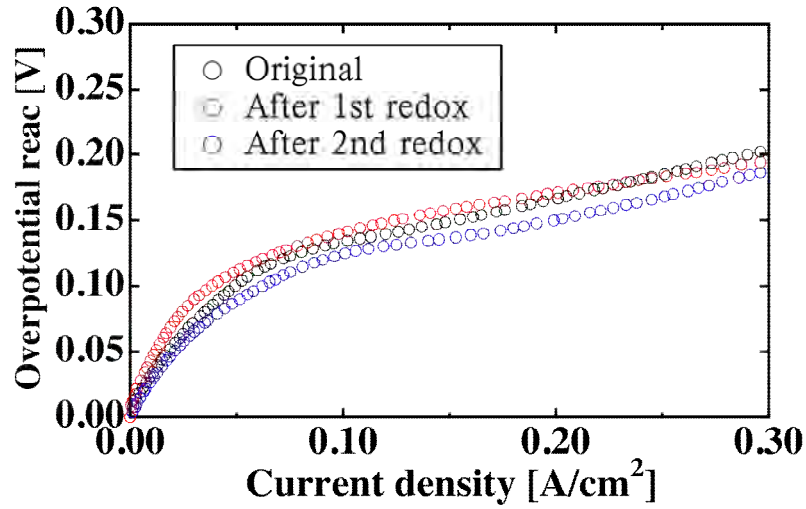

Fig.5 Schematic diagram of FIB-SEM measurement.

Fig.6 Measured overpotential of experiment A.
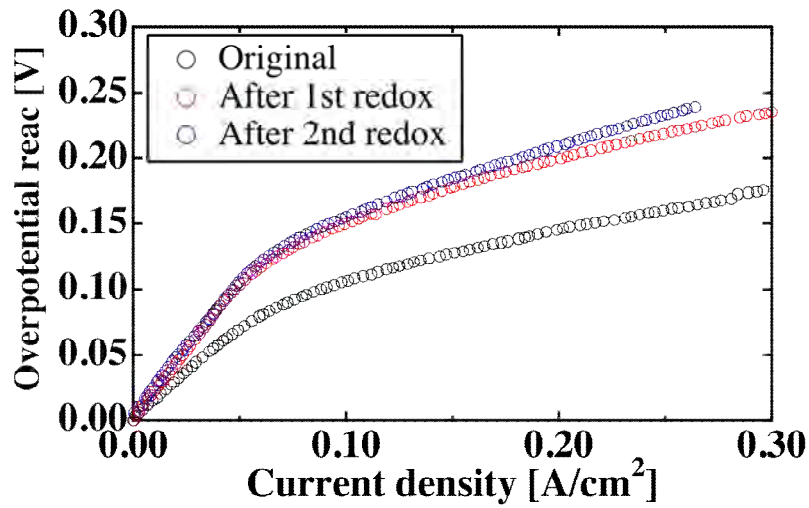
Fig.7 Measured overpotential of experiment B.
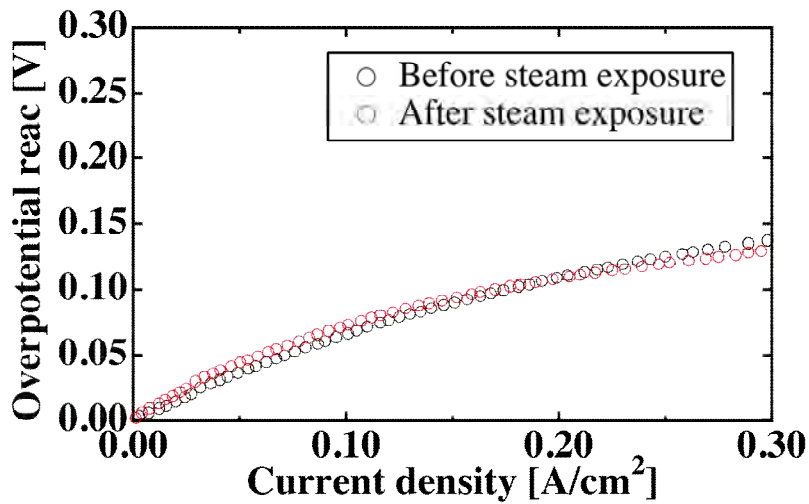
Fig.8 Measured overpotential of experiment C.
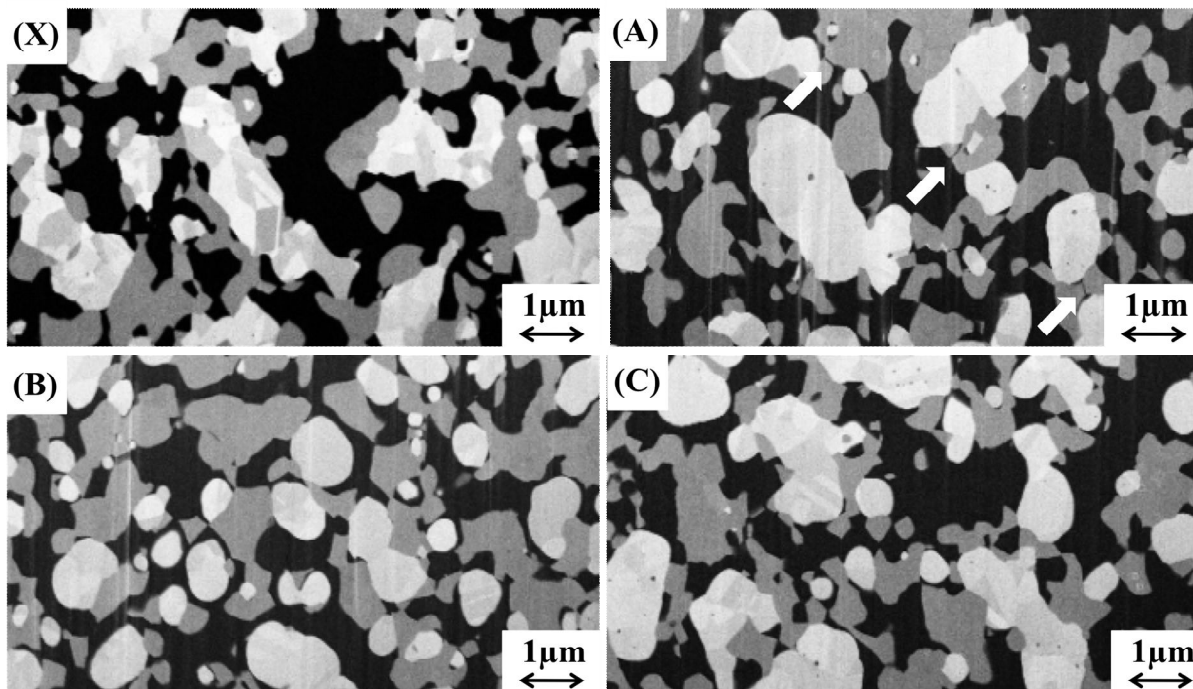
Fig.9 Cross sectional SEM images of the samples. Light gray is Ni, dark gray is YSZ and black is pore.
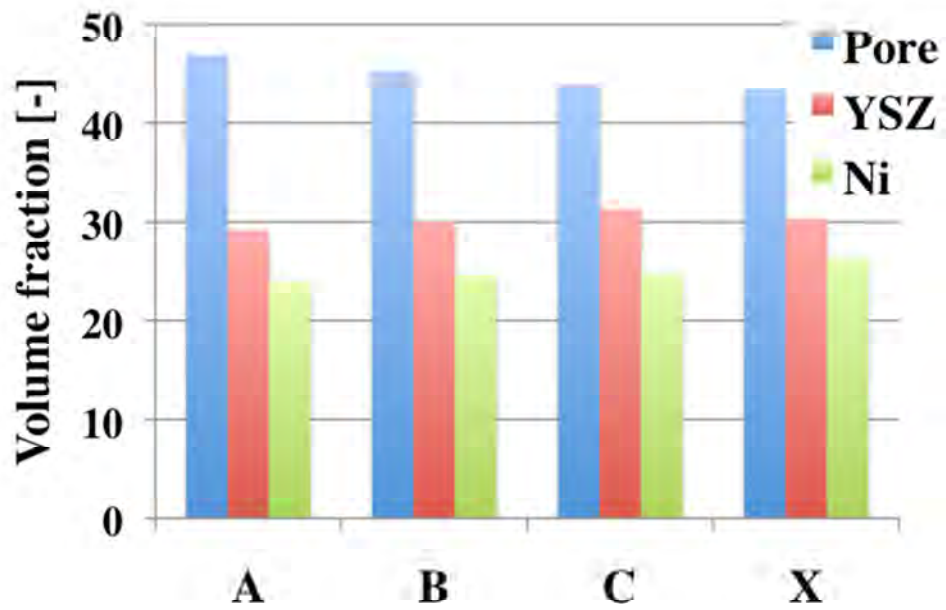
Fig.10 Volume fractions of the samples.
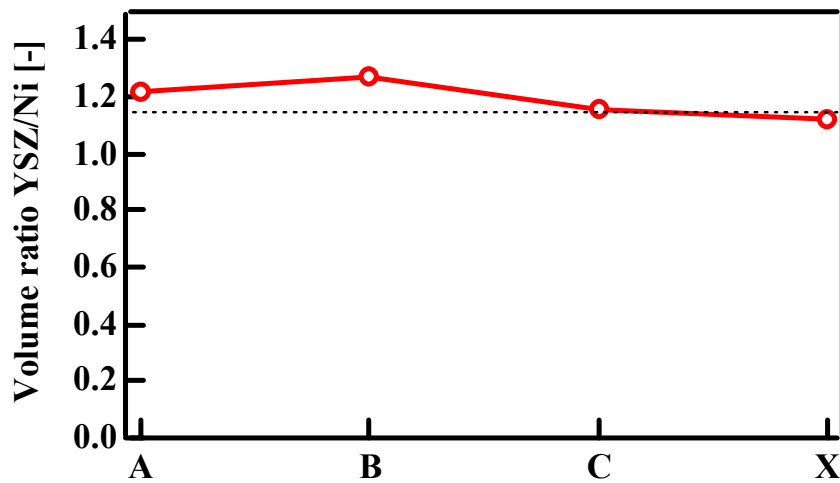
Fig.11 Volume ratio of YSZ and Ni.
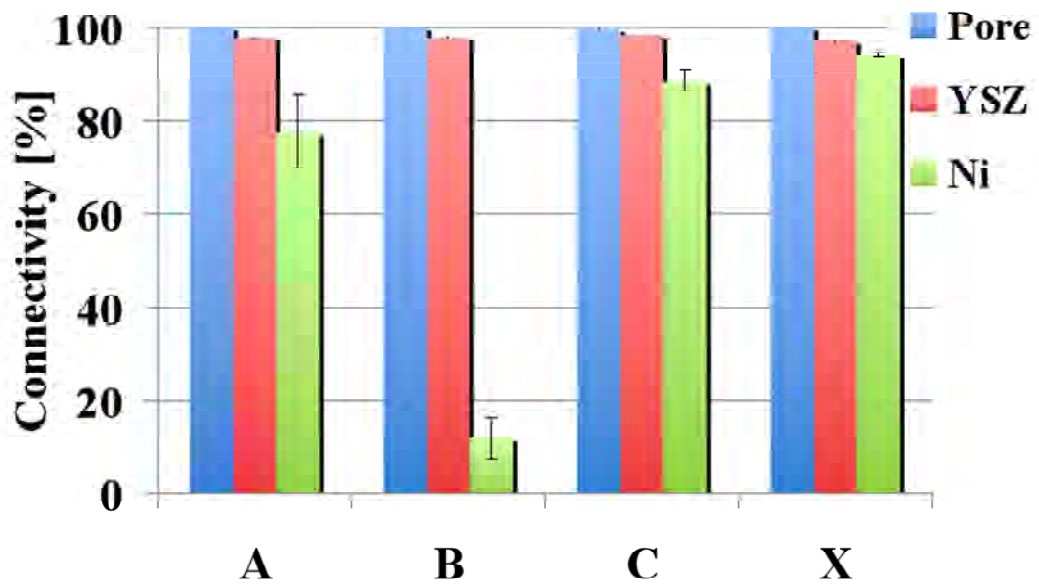
Fig.12   Connectivity of the phases.
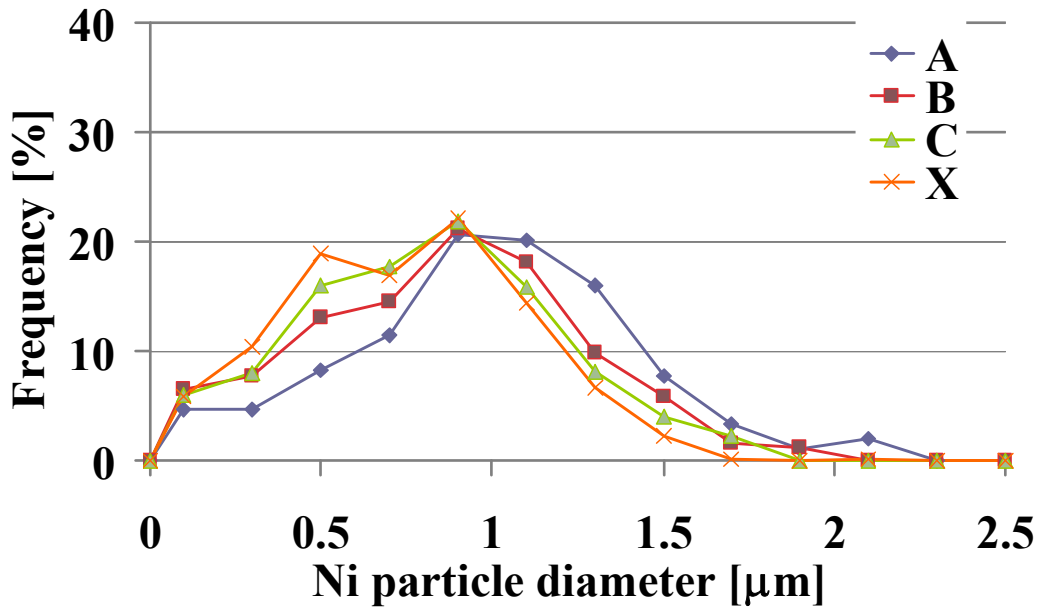
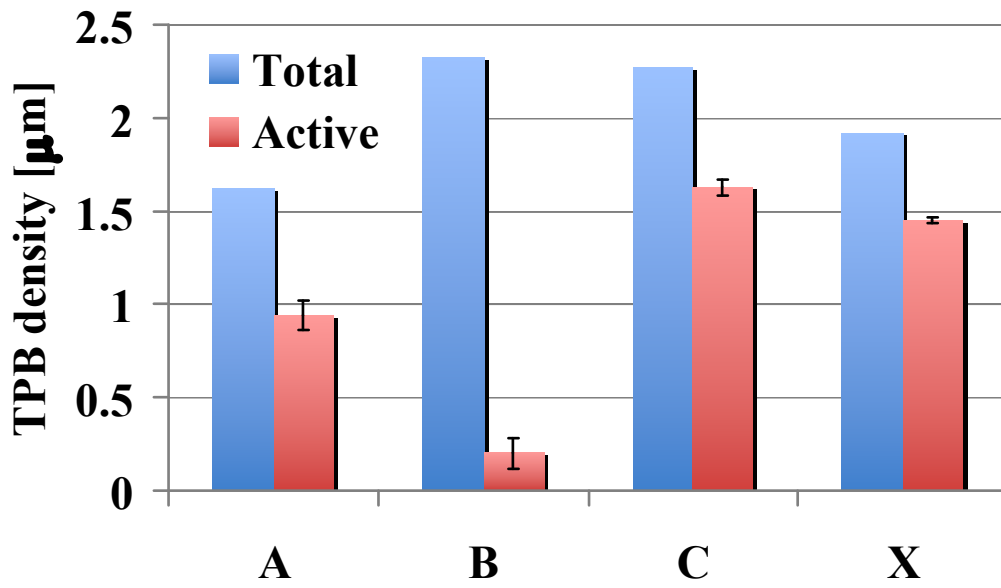Fig.13　Ni particle diameter.
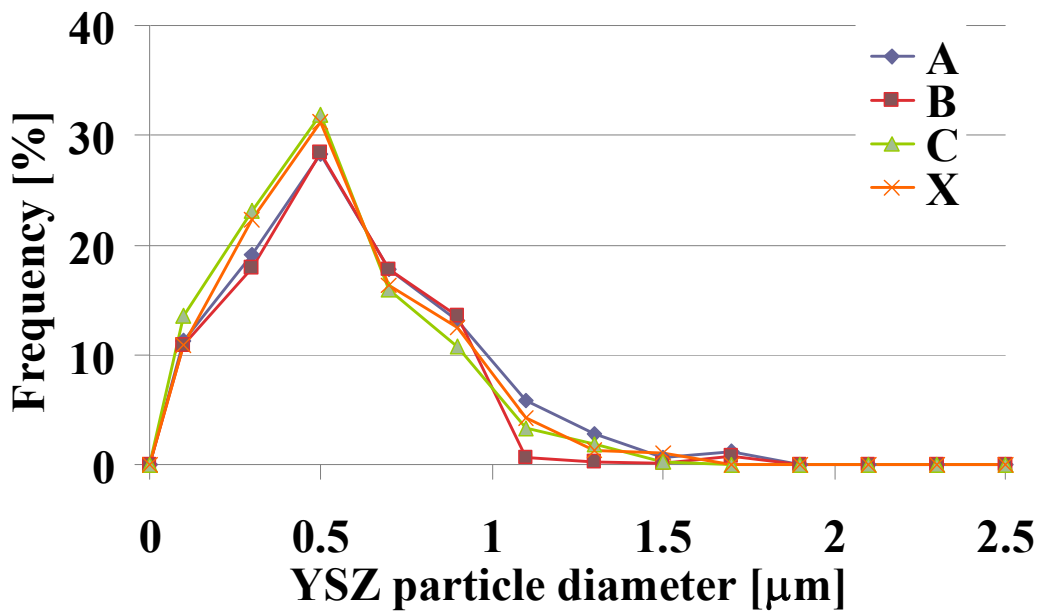
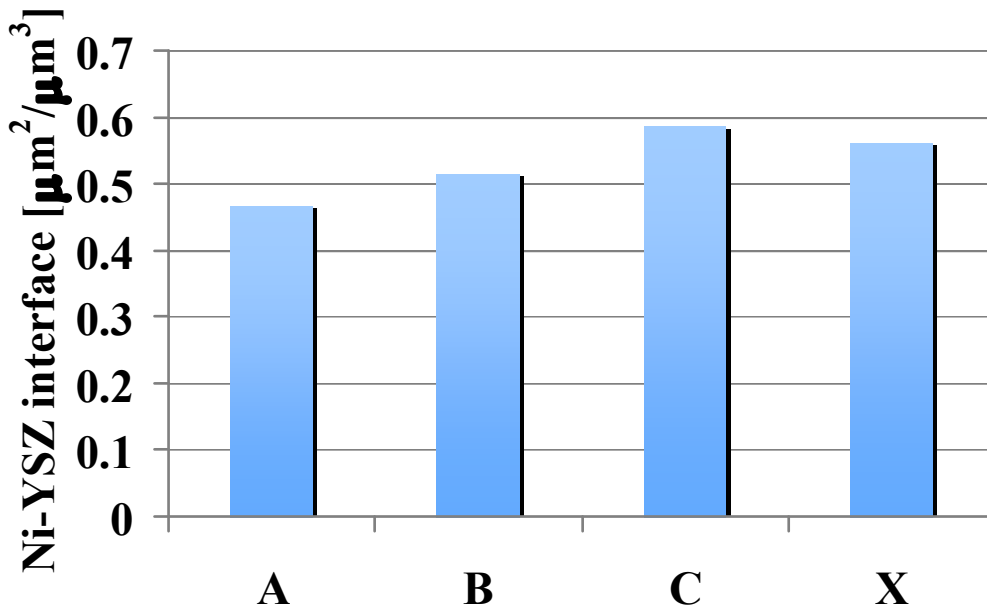Fig.14　YSZ particle diameter.

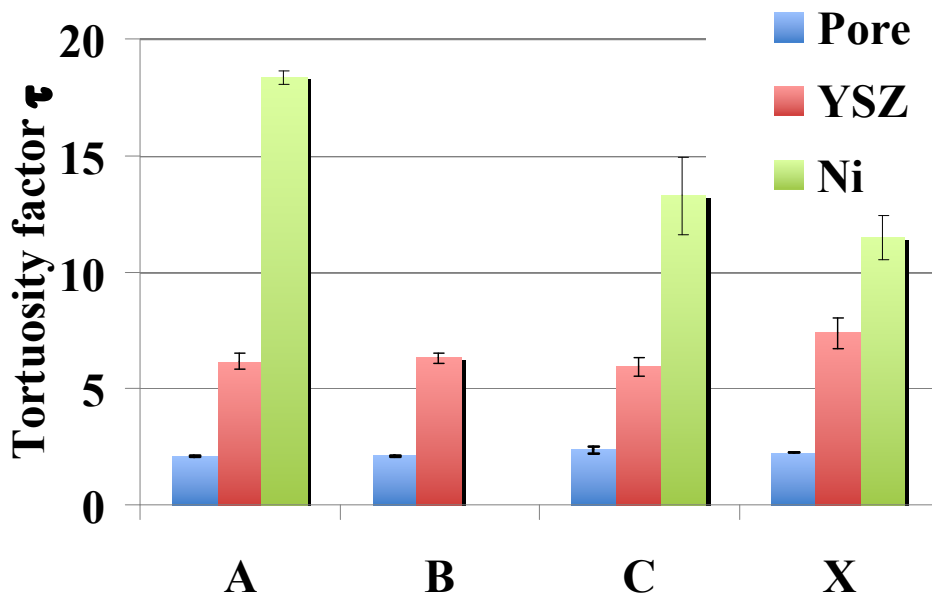Fig.15   TPB density.
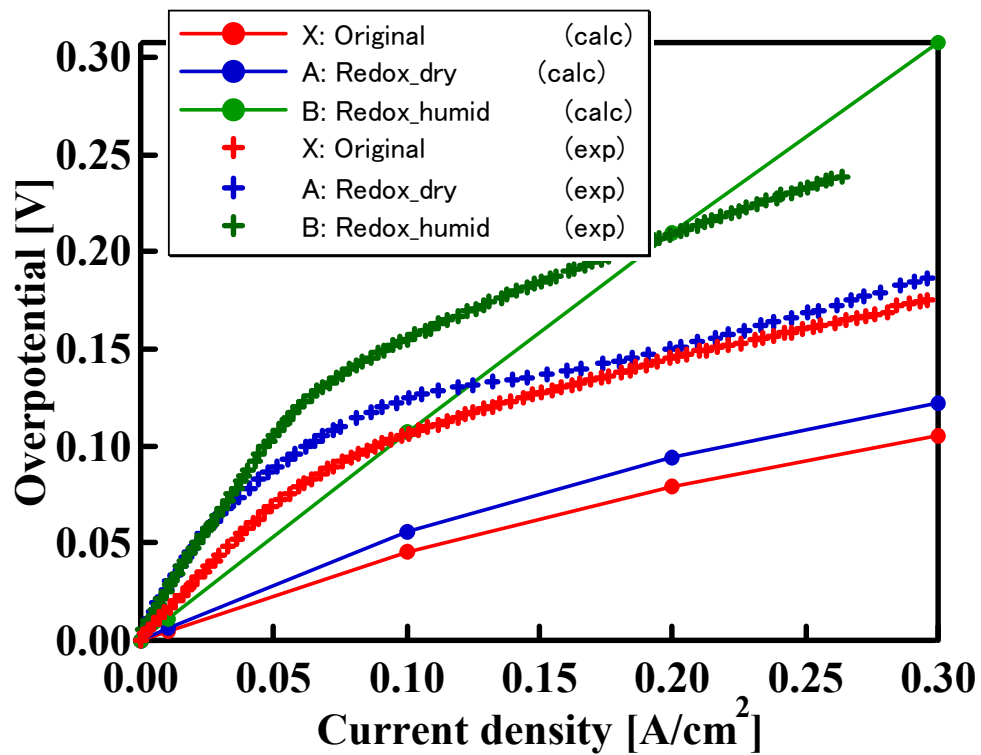

Fig.16 Ni-YSZ interface area.

Fig.17   Tortuosity factor.

Fig.18 Comparison between measured and calculated overpotentials.